Reconfigurable Delay Time Polymer Planar Lightwave Circuit for an X-band Phased-Array Antenna Demonstration

Brie Howley, Xiaolong Wang, Maggie Chen, and Ray T. Chen, *Fellow, IEEE*

***Abstract*—A 4-bit polymer optoelectronic true-time delay (TTD) device is demonstrated. The planar lightwave circuit (PLC) is composed of monolithically integrated low-loss passive polymer waveguide delay lines and five cascaded 2 × 2 polymer thermooptic switches. Waveguide junction offsets and air trenches simultaneously reduce the bending loss and device area. Simulations are used to optimize the trench and offset structures for fabrication. The 16 time delays generated by the device are measured to be in the range from 0 to 177 ps in 11.8-ps increments. The packaged PLC has an insertion loss of up to 14.9 dB, and the delay switching speed is 2 ms. An eight-element X-band phased-array antenna system is constructed to demonstrate the beam-steering capabilities of the 4-bit-delay devices. The TTD devices are shown to steer the far-field radiation pattern between 0° and −14.5°.**

***Index Terms*—Delay effects, integrated optoelectronics, phased arrays, planar waveguides, plastics, waveguide bends, waveguide switches.**

I. Introduction

OPTICAL FIBER and waveguide transmission lines are excellent candidates for the transmission and control of RF signals in future wide-bandwidth phased-array antenna (PAA) systems. Optical waveguides and fiber provide low propagation loss of RF and microwave signals, immunity to electromagnetic interference, and reduced system size and weight. They also remove the beam squint effect caused by highly dispersive electrical delay lines [1].

In contrast to fiber delay lines, waveguide optical delay lines, defined by the photolithographic methods, are able to deliver precise delays with subpicosecond resolution for PAA systems. Additionally, optical waveguide delay lines can be formed in a compact planar lightwave circuit (PLC) with waveguide optical switches. This technique has the potential for occupying less space than systems using optical fibers, Micro Electrical Mechanical Systems (MEMSs), or acoustooptic-based delay systems.

Several material systems have been used to fabricate waveguide optical delay lines, the most notable being lithium niobate [2], silica [3], silicon on insulator [4], and polymers [5]. In comparison with the alternative material systems, polymer waveguides are easy to fabricate on almost any substrate of interest [6], which reduces manufacturing costs and opens the possibility of single chip integration with active PAA components such as lasers, modulators, and detectors. Additionally, the thermooptical coefficient $\Delta n/\Delta T$ of polymer materials can be more than an order of magnitude greater than that of SiO_2 [7], enabling polymer thermooptic switches with power consumptions less than silicon- or oxide-based devices [8].

Low-refractive-index contrast waveguide material systems such as polymers can provide low propagation losses and low fiber to waveguide coupling losses by matching the numerical aperture and mode field diameters of the fibers and waveguides. However, a major drawback of any low-index contrast system for a PLC application is the large footprint that is attributable to the requirement of a large waveguide bend radius for low loss [9]. Polymers have the advantage of a widely tunable refractive index [10], but this still leaves a compromise between coupling and bend losses. The large bend radii requirement for low-index contrast systems is not practical for devices requiring large-scale integration such as optical delay lines and is detrimental to the device yield.

Air trenches have been proposed to reduce the radii by increasing the index contrast of a curved waveguide segment [11]–[14]. By increasing the index contrast within the waveguide bend region, the mode is tightly confined in order to prevent bend radiation losses without significantly affecting the propagation losses. Another modification to the waveguide design used to decrease bending losses is the offset. Waveguide offsets shift straight waveguide segments laterally with respect to the curved waveguides to decrease the mode mismatch [15], [16]. This, in turn, minimizes the junction loss between the curved and linear waveguide segments.

A 2-bit integrated polymer delay unit, containing two 2 × 2 optical switches, was previously reported with delays of 0, 37.8, 160.4, and 199.2 ps and an insertion loss less than 10 dB [17]. This device used digital optical switches and a combination of polymer waveguides and glass optical fibers and therefore suffered from delay inaccuracy and large device size.

Manuscript received May 2, 2006; revised August 23, 2006. This work was supported by the Navy SPAWAR, AFRL, AFOSR, DARPA, and NSF NNIN programs.

B. Howley was with the Microelectronics Research Center, University of Texas at Austin, Austin, TX 78758 USA. He is now with the MIT Lincoln Laboratory, Massachusetts Institute of Technology, Lexington, MA 02420 USA (e-mail: brie@ll.mit.edu).

X. Wang and R. T. Chen are with Microelectronics Research Center, University of Texas at Austin, Austin, TX 78758 USA (e-mail: wangxl@mail.utexas.edu; raychen@uts.cc.utexas.edu).

M. Chen is with Omega Optics, Austin, TX 78758 USA (e-mail: maggie.chen@omegaoptics.com).

Color versions of one or more of the figures in this paper are available online at http://ieeexplore.ieee.org.

Digital Object Identifier 10.1109/JLT.2006.890459

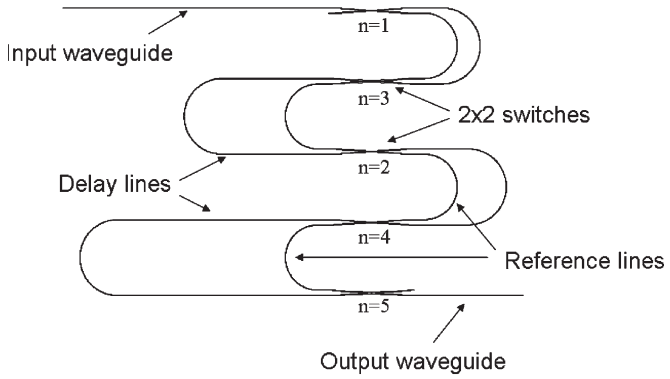

Fig. 1. TTD device structure employing waveguide optical switches and delay lines.

This paper reports on the design and demonstration of a packaged 4-bit true-time delay (TTD) device composed of monolithically integrated polymer waveguide delay lines and five 2×2 polymer total internal reflection (TIR) thermooptic switches. By using air trenches and waveguide offsets, the insertion loss of the reported TTD device is reduced by 2 dB, while the device size is reduced by 50%, when compared to a similar device structure without trenches or offsets. This is the first report on a polymer optical waveguide device that effectively uses trench and offset structures. Full characterization results of the TTD device are presented. Additionally, an X-band PAA system is constructed to demonstrate the beam-steering performance of the TTD devices.

II. Design and Fabrication of a 4-bit-Delay Device

A. Device Structure

An optical TTD device structure is described, which provides the required time delays to each element of a PAA subarray. The TTD device structure is based on the thermooptic polymer switches and polymer waveguide delay lines. The structure for the waveguide TTD device is shown in Fig. 1. A single-mode input waveguide is coupled to a 2×2 optical switch $(n = 1)$. Two different lengths of polymer waveguides are positioned at the output ports of the $n = 1$ switch. Depending on whether the bar state or cross state of the $n = 1$ switch is chosen, light is delivered to a waveguide reference line with length L or a waveguide delay line with length $L + \Delta L$. The outputs of these waveguides are connected to another 2×2 optical switch, and the switch's output ports are coupled to two more waveguides. This sequence is continued with lengths of the reference waveguides remaining at a length of L and the waveguide delay lines increasing in length according to $L + \Delta L \cdot 2^{(n-1)}$. The time delay increment Δt_n provided by each waveguide delay line is given by

$$\Delta t_n = \frac{2^{(n-1)} \cdot \Delta L \cdot n_g}{c} \tag{1}$$

where c is the speed of light in vacuum and n_g is the group index of the waveguide. The last switch $(n = 5)$ of the 4-bit-delay device is controlled to deliver the optical signal to the output waveguide. A key feature of this device structure is the layout of the delay lines, which are each composed of two straight segments of the appropriate length connected by a single 180° bend. This design minimizes the total length of the curved waveguides, thereby minimizing the total amount of the device bending loss.

TABLE I
Delay State Requirements for Each Element

	Element (n)							
Steering Angle (deg)	**1**	**2**	**3**	**4**	**5**	**6**	**7**	**8**
0	0	0	0	0	0	0	0	0
-14.5	7	6	5	4	3	2	1	0
14.5	0	1	2	3	4	5	6	7
-30	14	12	10	8	6	4	2	0
30	0	2	4	6	8	10	12	14

The base time delay increment Δt_1 was chosen as 11.8 ps in order to provide steering angles for an eight-element linear X-band array of -30°, -14.5°, 0°, $+14.5^\circ$, and $+30^\circ$. Table I lists the delay increments for each element as a function of the designed steering angle.

B. TIR Optical Switches

TIR optical switches are used in the TTD devices to redirect light to the desired optical delay line. Among various PLC switch architectures, TIR switches have the merits of compact size, wavelength insensitivity, polarization independence, and multimode tolerance [18], [19]. Details of the 2×2 TIR optical switch working principles and performance are mentioned in previous publications [20]–[22].

The tested TIR switch has a crosstalk of -31 dB in the cross state and a power consumption of 0 mW. The zero static power consumption is a beneficial feature since it can reduce the average driving power. With an increase in electrical driving power, the optical power in the cross port decreases, while the bar port optical power increases until the switch eventually reaches the bar state. The bar state power consumption is the driving power resulting in maximum optical power in the bar port, which is 44 mW, while the bar state crosstalk is -32 dB.

The switching time of the TIR switch is determined by the thermal conductivity and thickness of the polymer. The total polymer thickness is 21 μm. The optical switch exhibits rise and fall times of 1.5 and 2 ms, respectively. The total insertion loss of the fabricated switch with a fiber input and output was 2.8 dB in the bar state and 3.4 dB in the cross state. The variation in the insertion loss values is due to the interaction of the light with the X junction and thermal gradient induced by the heater. The reflection of light from the thermal gradient causes less scattering than when the light passes directly through the X junction. The TIR switch length was 4.9 mm, and the polarization-dependent loss (PDL) was measured to be less than 0.2 dB in either switch state.

C. Structures for Waveguide Bend Loss Reduction

Simulation and experimental loss measurements have shown that trenches are effective structures for preventing bend radiation losses in low-refractive-index contrast optical waveguides and waveguide offsets can improve optical coupling of the

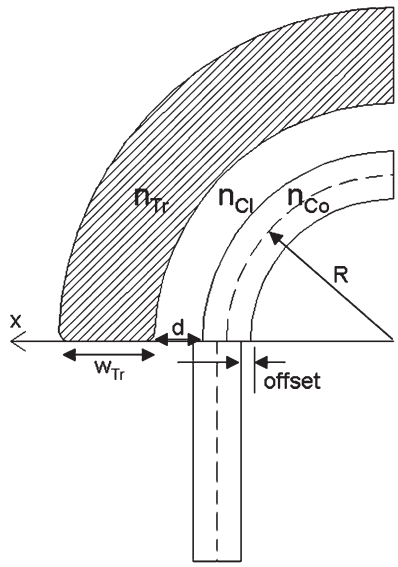

Fig. 2. Diagram of the waveguide core using offset and trench (hatched area) structures.

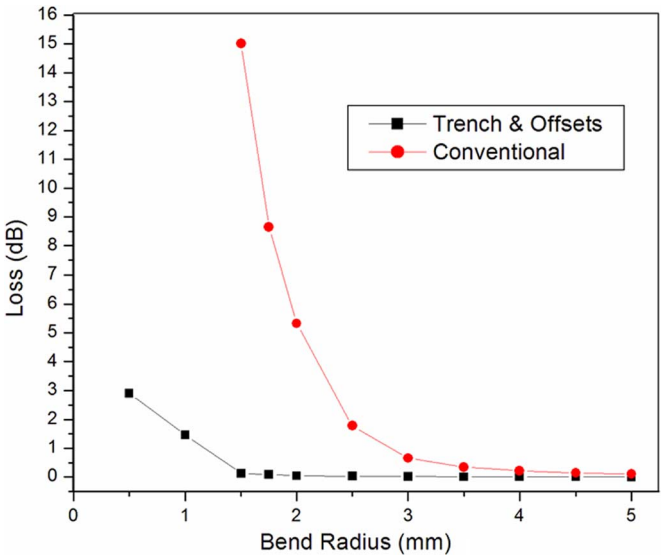

Fig. 4. Simulated bend and junction losses for the 180° waveguide bends ($d = 7$ μm).

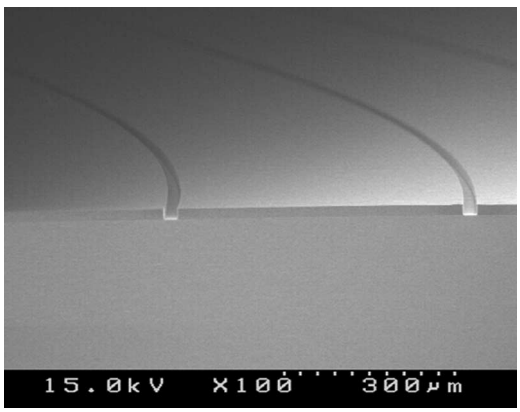

Fig. 3. SEM image of the waveguide with trench cross section.

straight and curved waveguide segments [23]. Waveguide trench and offsets were designed to reduce the TTD device size and to minimize the bend loss of the waveguide delay lines.

1) Trenches: A curved waveguide with an air trench structure is a relatively simple way to confine the mode through the bend. Fig. 2 illustrates a top view of a step index channel waveguide junction between the straight and curved waveguide segments. The structure utilizes both an air trench ($n_{\mathrm{Tr}} = 1$) and an offset. The core and cladding indexes are n_{Co} and n_{Cl}, respectively, and the waveguide has a bend radius of R. The width of the trench w_{Tr} and the separation between the inside radius of the trench and the outside radius of the waveguide core d are also labeled. By placing the air trench sufficiently close to the waveguide core, (reducing d) the waveguide mode is confined, the evanescence tail is reduced, and a decreased bend loss is expected. Simulation and experimental results [23] suggest that a trench separation of 7 μm provides adequate confinement of the mode while allowing an acceptable amount of alignment tolerance for the fabrication procedure. Fig. 3 is a cross-sectional SEM image of polymer waveguides with air trenches.
2) Offsets: In a straight channel waveguide, the electric field intensity pattern of the fundamental mode is symmetric about the center of the waveguide core. In contrast, the fundamental mode in a curved waveguide, with the same core cross section, has the field peak displaced laterally toward the outside of the bend, and the mode is asymmetric, with a width different from that of the straight waveguide. Because the mode fields are mismatched, transition losses will occur at the junction of two waveguides with different radii, causing a reduction in the power transfer between the two waveguides. A lateral offset at the junction of the two waveguides may be used to reduce the mode mismatch.
3) Simulations: The 3-D semivectorial beam propagation method (BPM) simulations [24] were performed to determine the optimal trench and offset design, with the goal of minimizing the waveguide bend radius while suffering an acceptable amount of bend and junction losses. As a comparison, the bend loss was also simulated for a conventional waveguide not using trench or offset structures. All simulations were based on core and cladding materials with refractive indexes of 1.460 and 1.450, respectively, and the core was 6.5 $\times$ 6.5 μm^2 in order to maintain a single-mode behavior at the wavelength of 1.55 μm. The simulation conditions assumed a trench width (w_{Tr}) of 20 μm and a trench separation (d) of 7 μm. The 180° bends were simulated with a BPM equivalent index transformation in order to avoid paraxial effects. This method has been shown to be accurate for bends with radii much greater than the core width dimension [15]. Mode overlap integrals were performed to determine the optimum offset distance and junction loss between straight and curved waveguide sections as a function of waveguide bend radius.

Fig. 4 shows the results of these simulations. For the waveguide not utilizing offsets or trenches, there is an exponential increase in the bend loss as the radius decreases. However,

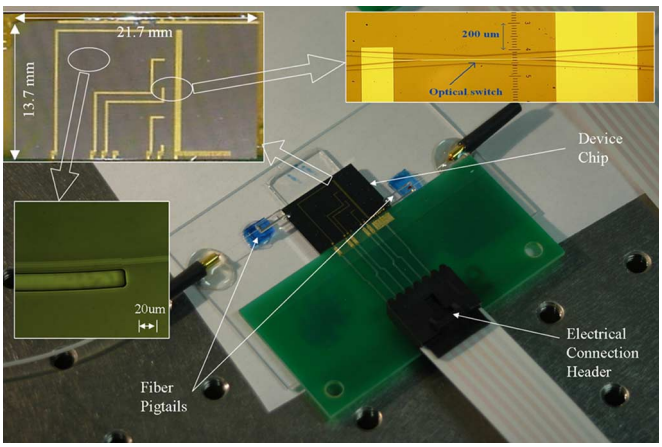

Fig. 5. Photograph of a packaged 4-bit TTD device.

for the waveguide with trenches and offsets, there is a notable improvement in the loss for the bend radii less than 3 mm. Between approximately 1.5 and 3 mm, the loss remains flat. The 90% transmission values for the 180° bends occur at the bend radii of approximately 3.3 mm for the conventional waveguide and 1.4 mm for the waveguide utilizing trenches and offsets.

D. Fabrication Procedure

Polymer waveguides were fabricated using a UV curable perfluorinated acrylate material on a silicon wafer. The refractive index of the core and cladding materials after curing was 1.459 and 1.449, respectively. The channel waveguide cores, which are 6.5-μm wide by 6.5-μm tall, were formed by reactive ion etching (RIE). The waveguides exhibited a single-mode behavior with a measured propagation loss of 0.45 dB/cm at the wavelength of 1.55 μm. The core mask layer contained input/output waveguides and optical switch structures, as well as delay and reference lines with offsets at the boundary between the straight and curved waveguide sections. The reference and delay lines used waveguide bend radii of 1.5 and 1.75 mm, respectively. Once the waveguide layer was formed, a gold film was deposited and patterned to form the electrodes' structures for the switches. A SiO_2 hard mask was deposited by plasma enhanced chemical vapor deposition and patterned with RIE to form the trench windows. The cladding material in the trench area was then removed with RIE.

The wafer supporting the TTD devices was then diced, and optical fibers were aligned and attached to the input and output waveguides with optical epoxy. The optical assembly was mounted on a custom-designed PC board, and gold wire bonding was used to form electrical connections from the board to the switches in the TTD device. A soldered electrical connector on the board provided the external electrical interface to the device chip. Fig. 5 is a photograph of a packaged TTD device. An inset in Fig. 5 shows a photograph of the device chip. The TTD device is 21.7-mm long by 13.7-mm wide. A high magnification view of an optical switch and a waveguide bend with a trench and offset are also shown as insets in Fig. 5.

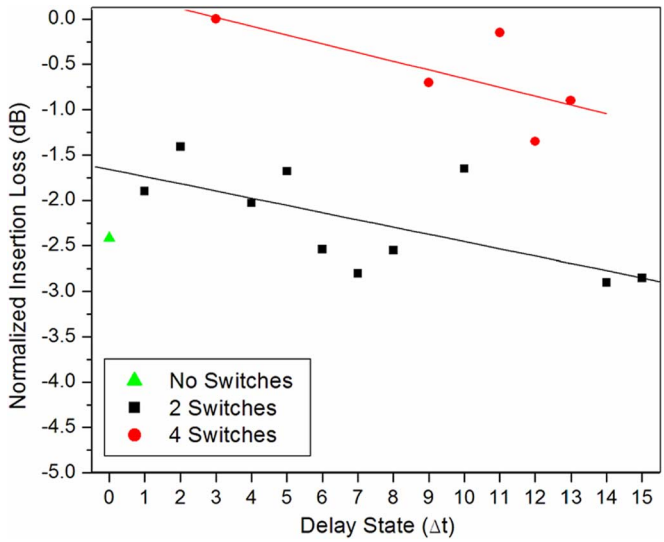

Fig. 6. Normalized insertion loss as a function of the delay state.

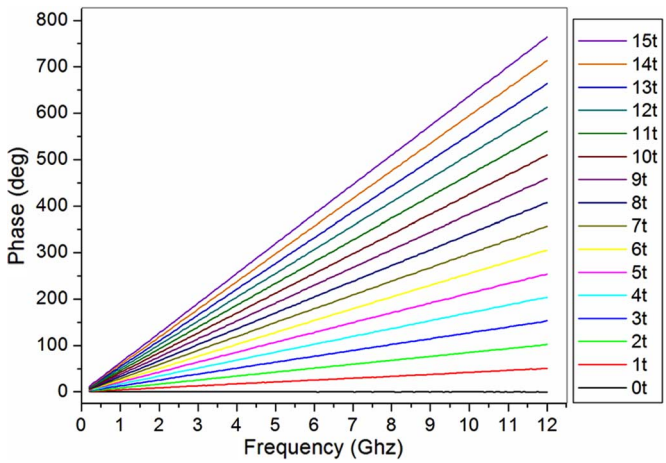

Fig. 7. Measured phase versus frequency response for each delay state.

III. Results of 4-bit-Delay Device Performance

To evaluate the performance of the fabricated delay device, the insertion loss of a fully packaged 4-bit-delay device was measured for each of the delay states. The insertion loss of the shortest delay state $0\Delta t$ was 14.5 dB. The PDL was measured as 0.64 dB, with the transverse magnetic (TM) polarization having a lower loss than transverse electric (TE). The insertion losses of the other delay states were each measured individually. Fig. 6 shows the normalized insertion loss as a function of the delay state for a randomly polarized input signal. The overall variation in insertion loss was 2.9 dB, with $3\Delta t$ having the lowest insertion loss. Delay states with four switches activated had higher throughputs than those states with just two or no switches activated. In addition, larger delays also had lower throughputs.

The insertion loss of the TTD device was expected to be dependent on the delay state. Although relatively low, the propagation loss of the polymer waveguide was not negligible. Consequently, longer path lengths induced higher losses. In addition, as was noted previously, the insertion loss of the TIR

TABLE II
DESIGNED AND MEASURED DELAY VALUES FOR EACH DELAY STATE

Delay State (Δt)	Switches Activated	Designed Delay Value (ps)	Measured Delay Value (ps)
0	none	0	-0.04
1	1,2	11.8	11.7
2	3,4	23.6	23.5
3	1,2,3,4	35.4	35.4
4	2,3	47.2	47.4
5	1,3	59	59.1
6	2,4	70.8	70.9
7	1,4	82.6	82.7
8	4,5	94.4	94.4
9	1,2,4,5	106.2	106.2
10	3,5	118	118.0
11	1,2,3,5	129.8	129.8
12	2,3,4,5	141.6	141.8
13	1,3,4,5	153.4	153.6
14	2,5	165.2	165.1
15	1,5	177	176.9

switch was also dependent on the switch state activated, with the bar port states having roughly 0.6 dB lower loss than the cross port state. Therefore, delay states with more switches activated in the bar state (heater turned on) were expected to have lower loss than delay states with fewer switch heaters turned on. Lines fitted to the data in Fig. 6 help to show the trend in the insertion loss as a function of the number of switches activated. The slope of these lines can be correlated to the propagation loss of the polymer waveguides.

The delay values of the packaged 4-bit TTD device were measured. A CW laser, operating at 1.55 μm, was modulated by a $LiNbO_3$ modulator fed by an HP8510C network analyzer. The output of the modulator was the input to the delay device. An erbium-doped fiber amplifier (EDFA) was used to amplify the signal. A photodetector (PD) covering the X-band frequency range was used to convert the modulated optical signal to an electrical signal that was fed back to the network analyzer.

Fig. 7 shows the measured phase versus frequency data values for all delay states. Each set of data is composed of 201 measurement values. The linear response for each data set is indicative of the TTD effect. The delay values were derived from the slope of a linear regression fit for each respective measured data set. Table II lists the switches that were activated to produce each delay state and the designed and measured delay values. There is only as much as 0.2-ps variation between any of the measured and designed values. The error of the delay measurement was determined to be as large as ± 0.8 ps.

The difference in the delay between TM and TE polarized signals was measured for the shortest and longest delay paths. A half-wave plate, used to rotate the TM polarization into a TE polarization, was inserted in the delay measurement system before the delay device. The polarization delay difference of the measurement system, without the TTD device, was also measured and found to be -1.74 ps. The TTD device contribution to the polarization delay difference (TM–TE) was 0.36 and 0.30 ps for the longest and shortest delay states, respectively. These values are both less than the delay measurement error, and so, it can be deduced that the polarization delay difference is negligible.

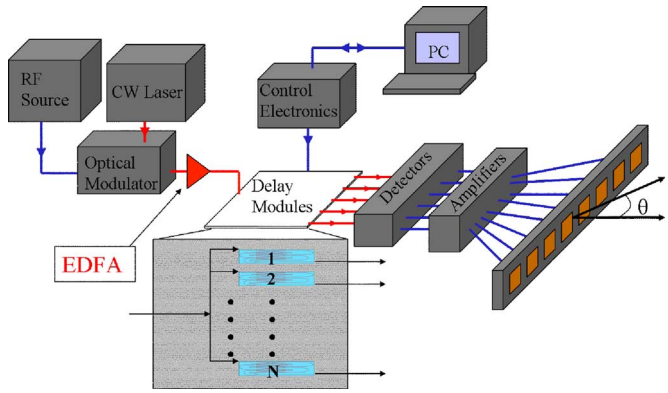

Fig. 8. Diagram of the optically controlled linear PAA system.

IV. ANTENNA ARRAY DEMONSTRATION

A PAA system was constructed to demonstrate the beam-steering capability of the 4-bit TTD devices. The 1×8 linear array system structure is shown in Fig. 8. A laser supplied the carrier wave for the optical delay system. The continuous wave laser was modulated with a 40-Gb/s optical modulator. The analog microwave signal driving the modulator was provided by an HP8510C network analyzer. The modulated optical signal was then amplified with an EDFA and split with a 1×8 optical splitter. The optical signals were then fed to the programmable 4-bit TTD devices, which delayed the optical signals by the appropriate values for a predetermined antenna steering angle. The delayed optical signals were then inputted to a set of PDs that converted the modulated optical signal into an analog electrical signal. The delayed microwave signals were then amplified and fed to an X-band array of patch antenna elements with 1.4-cm spacings. The delay paths for each element were equalized, as described by Shi *et al.* [25]. Fig. 9 is a photograph of the constructed optically controlled PAA system.

A horn antenna, located in the far-field region, received the propagating microwave signal, and a microwave frequency spectrum analyzer measured the intensity and frequency radiated by the antenna array. To measure the far-field pattern, the

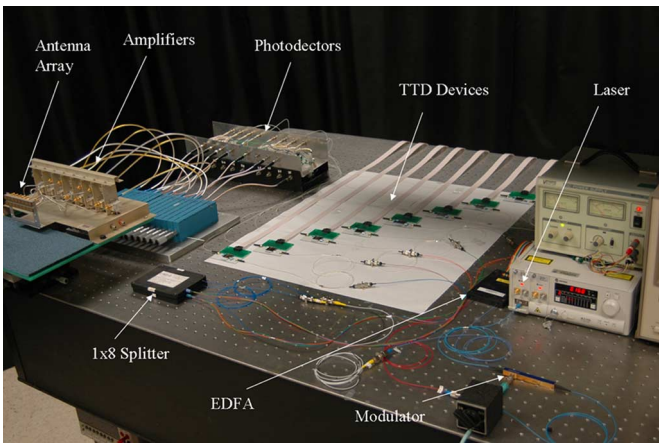

Fig. 9. Photograph of the optically delayed PAA system.

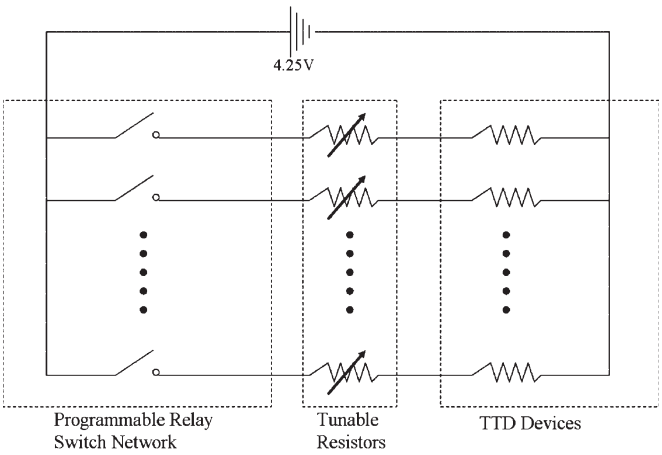

Fig. 10. Schematic of the electrical circuit used to control the optical switches.

antenna array was rotated by a computer-controlled rotational stage, and the received microwave signal intensity was recorded at designated angles. The rotational stage was limited in movement to angles between -30° and $+30^\circ$.

A computer-controlled relay switch network simultaneously controlled the switching state of all the optical switches in the TTD devices. Fig. 10 is a schematic of the electrical circuit. A single power supply, with a fixed voltage of 4.25 V, provided the current for all the eight devices. The power supply was connected to the common line of the relay switch network. Each relay switch was connected in series with a tunable resistor and one of the optical switches in the TTD devices. The thin-film heaters of the TIR optical switches are represented by a pure resistance in Fig. 10. These heaters were connected in parallel, and the return line was connected to the ground of the power supply. The tunable resistors were required to compensate for variations of the optical switch heater resistance introduced by the TTD device fabrication procedure.

For a predetermined steering angle, the appropriate relay switches were programmed to close the circuit of each switch, causing a current to flow through the corresponding tunable resistor and thin-film heater. This activated the associated optical switches, allowing the optical signal to travel through the desired delay path.

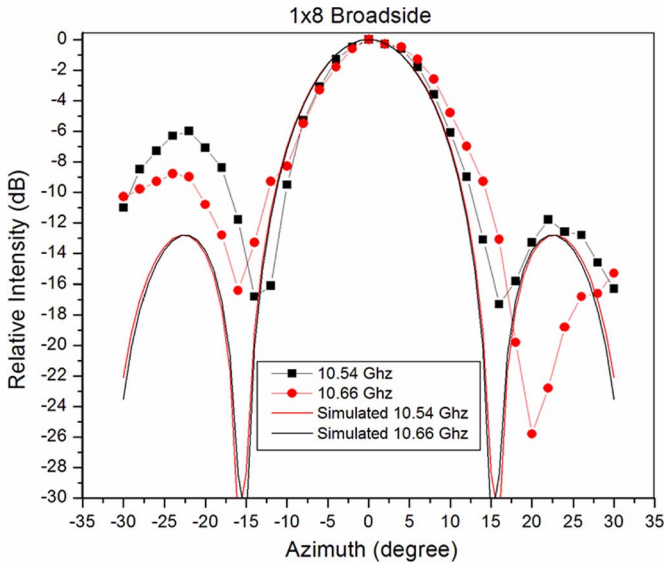

Fig. 11. Measured and simulated far-field patterns for a 1×8 element array (0° steering angle).

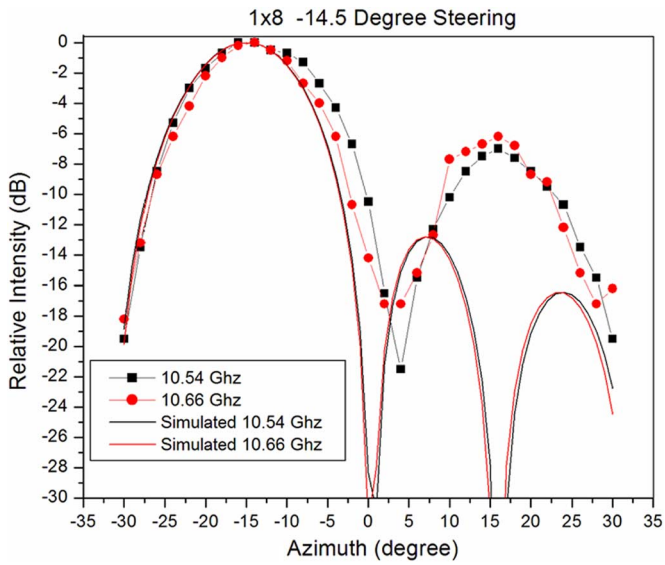

Fig. 12. Measured and simulated far-field patterns for a 1×8 element array (-14.5° steering angle).

The greatest benefit of a PAA system using optical TTD is the large instantaneous bandwidth. Ideally, a system demonstration of an optically controlled X-band antenna array would be expected to show no beam squint effects across the entire X-band spectrum (8–12 GHz). However, the patch antenna elements in this system demonstration had an inherently narrow bandwidth. Consequently, only frequencies of 10.54 and 10.66 GHz had an adequate signal to noise ratio for the microwave spectrum analyzer to detect the transmitted signal.

The antenna steering angles listed in Table I were each confirmed by the measurement of the far-field radiation patterns. Fig. 11 shows the simulated and measured broadside far-field patterns for an eight-element linear array. The full-width at half-maximum of the main beam is approximately 14°. The peak is clearly distinguishable at 0° for both 10.54- and 10.66-GHz

frequencies. The first side lobe peaks should ideally occur at -13 dB, but the measured results show asymmetric side lobes. This was found to be attributable to nonuniform radiation efficiencies of the antenna elements.

Fig. 12 shows the simulated and measured far-field patterns for a 1×8 element array with a steering angle of -14.5°. As was the case with the broadside direction, the peak intensity is clearly distinguishable at the desired steering angle for both frequencies. However, the measured side lobe pattern does not conform to the simulated pattern. This is attributable to the nonuniform power radiated from the elements, as well as a possible multipath effect occurring from the power reflected off the walls in the room where the measurement was performed.

V. Conclusion

The design and measurement of an integrated polymer 4-bit optical TTD device has been presented. The device was composed of polymer waveguide delay lines and polymer 2×2 optical switches operating on a thermooptic-induced TIR effect. Trench and offset waveguide bend loss reduction structures were utilized to reduce the waveguide bend radius, resulting in a smaller device size.

A packaged 4-bit-delay device was measured for insertion loss uniformity, PDL, and delay accuracy. The fiber-to-fiber insertion loss of the device was 14.5 dB. While this loss is currently too large for real-world applications, it could be reduced by using lower loss polymer materials. The maximum variation of the insertion loss was found to be 2.9 dB, and the PDL was 0.64 dB. The optical switches are the largest contributor to the PDL of the device. Other polymer switch designs with lower PDLs are being evaluated to minimize the TTD device PDL. The measured delay values had less than 0.25-ps deviation from the designed delay values, and the polarization-induced delay differences were negligible. The response time of the device is dictated by the optical switch rise and fall times that were measured to be 1.5 and 2 ms, respectively. These response times could be decreased by reducing the polymer cladding thickness.

An optically controlled PAA system utilizing the 4-bit TTD devices was demonstrated. The 4-bit optical TTD devices provided the required delays to steer the antenna radiation pattern of an eight-element linear X-band array. Tunable resistors were used to ensure a low crosstalk of the optical switches in the TTD devices. Far-field patterns for a 1×8 X-band array were simulated and measured at frequencies of 10.54 and 10.66 GHz. The far-field measurements showed the correct beam-steering effect at angles of 0° and -14.5°.

References

[1] W. Ng, A. Walston, L. Tangonan, J. J. Lee, I. Newberg, and N. Bernstein, "The first demonstration of an optically steered microwave phased array antenna using true-time-delay," *J. Lightw. Technol.*, vol. 9, no. 9, pp. 1124–1131, Sep. 1991.

[2] E. Voges, K. Kuckelhaus, and B. Hosselbarth, "True time delay integrated optical RF phase shifters in lithium niobate," *Electron. Lett.*, vol. 33, no. 23, pp. 1950–1951, Nov. 1997.

[3] K. Horikawa, I. Ogawa, T. Kitoh, and H. Ogawa, "Photonic integrated beam forming and steering network using switched true-time-delay silica-based waveguide circuits," *IEICE Trans. Electron.*, vol. E79-C, no. 1, pp. 74–79, Jan. 1996.

[4] S. Yegnanarayanan, P. D. Trinh, F. Coppinger, and B. Jalali, "Compact silicon-based integrated optic time delays," *IEEE Photon. Technol. Lett.*, vol. 9, no. 5, pp. 634–635, May 1997.

[5] S. Tang, B. Lin, N. Jiang, D. An, Z. Fu, L. Wu, and R. T. Chen, "Ultra-low-loss polymeric waveguide circuits for optical true-time delays in wideband phased array antennas," *Opt. Eng.*, vol. 39, no. 3, pp. 643–651, Mar. 2000.

[6] R. T. Chen, "Polymer-based photonic integrated circuits," *Opt. Laser Technol.*, vol. 25, no. 6, pp. 347–365, Dec. 1993.

[7] L. Eldada, "Optical communication components," *Rev. Sci. Instrum.*, vol. 75, no. 3, pp. 575–593, Mar. 2004.

[8] Y. Hida, O. Hidekatsu, and S. Imamura, "Polymer waveguide thermooptic switch with low electric power consumption at 1.3 μm," *IEEE Photon. Technol. Lett.*, vol. 5, no. 7, pp. 782–784, Jul. 1993.

[9] F. Ladouceur and J. D. Love, *Silica-Based Buried Channel Waveguides and Device*. London, U.K.: Chapman & Hall, 1996, ch. 10.

[10] L. Eldada, "Advances in telecom and datacom optical components," *Opt. Eng.*, vol. 40, no. 7, pp. 1165–1178, Jul. 2001.

[11] J. Yamauchi, M. Ikegaya, and H. Nakano, "Bend loss of step-index slab waveguides with a trench section," *Microw. Opt. Technol. Lett.*, vol. 5, no. 6, pp. 251–254, Jun. 1992.

[12] C. Seo and J. C. Chen, "Low transition losses in bent rib waveguides," *J. Lightw. Technol.*, vol. 14, no. 10, pp. 2255–2259, Oct. 1996.

[13] M. Rajarajan *et al.*, "Design of compact optical bends with a trench by use of finite-element and beam-propagation methods," *Appl. Opt.*, vol. 39, no. 27, pp. 4946–4953, Sep. 2000.

[14] M. Popovic, K. Wada, S. Akiyama, H. A. Haus, and J. Michel, "Air trenches for sharp silica waveguide bends," *J. Lightw. Technol.*, vol. 20, no. 9, pp. 1762–1772, Sep. 2002.

[15] L. Lerner, "Minimum bending loss interconnection for integrated optics waveguides," *IEEE Electron Device Lett.*, vol. 29, no. 9, pp. 733–735, Apr. 1993.

[16] T. Kitoh, N. Takato, M. Yasu, and M. Kawachi, "Bending loss reduction in silica-based waveguides by using lateral offsets," *J. Lightw. Technol.*, vol. 13, no. 4, pp. 555–562, Apr. 1995.

[17] B. Howley, Y. Chen, X. Wang, Q. Zhou, and R. T. Chen, "2-bit reconfigurable true time delay lines using 2×2 polymer waveguide switches," *IEEE Photon. Technol. Lett.*, vol. 17, no. 9, pp. 1944–1946, Sep. 2005.

[18] C. S. Tsai, B. Kim, and F. R. Akkari, "Optical channel waveguide switch and coupler using total internal reflection," *IEEE J. Quantum Electron.*, vol. QE-14, no. 7, pp. 513–517, Jul. 1978.

[19] J. Yang, Q. Zhou, and R. T. Chen, "Polyimide-waveguide-based optical switch using total internal reflection effect," *Appl. Phys. Lett.*, vol. 81, no. 16, pp. 2947–2949, Oct. 2002.

[20] X. Wang, B. Howley, M. Chen, and R. T Chen, "Polarization-independent all-wave polymer-based TIR thermooptic switch," *J. Lightw. Technol.*, vol. 24, no. 3, pp. 1558–1565, Mar. 2006.

[21] B. Howley, X. Wang, Y. Chen, and R. T. Chen, "Integrated polymer optoelectronic time delay device for an X-band phased array antenna system," *Proc. SPIE*, vol. 6124, pp. 283–295, Mar. 2006.

[22] M. Y. Chen, B. Howley, X. Wang, P. Basile, and R. T. Chen, "2-D scalable optical controlled phased-array antenna system," *Proc. SPIE*, vol. 6126, pp. 187–193, Feb. 2006.

[23] B. Howley, X. Wang, Y. Chen, and R. T. Chen, "Experimental evaluation of curved polymer waveguides with air trenches and offsets," *J. Appl. Phys.*, vol. 100, no. 2, p. 23 114, Jul. 2006.

[24] R. Scarmozzino, A. Gopinath, R. Pregla, and S. Helfert, "Numerical techniques for modeling guided-wave photonic devices," *IEEE J. Sel. Topics Quantum Electron.*, vol. 6, no. 1, pp. 150–162, Jan./Feb. 2000.

[25] Z. Shi, L. Gu, B. Howley, Y. Jiang, Q. Zhou, R. T. Chen, Y. Chen, X. Wang, H. R. Fetterman, and G. Brost, "True-time-delay modules based on a single tunable laser in conjunction with a waveguide hologram for phased array antenna application," *Opt. Eng.*, vol. 44, no. 8, p. 84 301, Aug. 2005.

Brie Howley received the B.S. degree in materials science from the University of Wisconsin–Madison, in 1998 and the Ph.D. degree in electrical engineering from the University of Texas at Austin, in 2006. His Ph.D. dissertation was centered on optically controlled wide-bandwidth phased-array antennas.

After graduation from the University of Texas, he joined Massachusetts Institute of Technology (MIT) Lincoln Laboratory, Lexington, MA, where he currently performs research and development of advanced radar systems. He has over 20 publications in peer-reviewed journals and conferences.

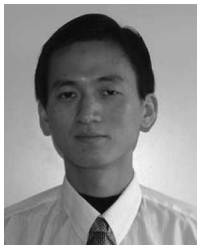

Xiaolong Wang received the B.S. degree in material science and engineering from Tsinghua University, Beijing, China, in 2000, the M.S. degree in electrical engineering from Chinese Academy of Sciences, Beijing, in 2003, and the Ph.D. degree in electrical and computer engineering from University of Texas at Austin, in 2006.

He is currently with the Microelectronics Research Center, University of Texas at Austin. His current research includes polymeric photonic devices for true-time delay and board-level optical interconnects.

Maggie Chen received the Ph.D. degree in electrical engineering, with specialization on optoelectronic interconnects, from University of Texas at Austin, in 2002.

She has served as a Principal Investigator for projects from the National Science Foundation (NSF) and Missile Defense Agency (MDA) and Commander for the Space and Naval Warfare Systems Command (SPAWAR), Defense Advanced Research Projects Agency (DARPA), National Aeronautics and Space Administration (NASA), and the Army. She is currently with Omega Optics, Austin. She has over 40 publications in refereed journals and conferences. Her research work in the past ten years has been focused on optical true-time delay feeding networks for phased-array antennas, planar waveguide devices, optoelectronic interconnects, and diffractive optical elements.

Dr. Chen is a member of The International Society for Optical Engineering (SPIE).

Ray T. Chen (M'91–SM'98–F'04) received the B.S. degree in physics from National Tsing-Hua University, Taiwan, R.O.C., in 1980 and the M.S. degree in physics and the Ph.D. degree in electrical engineering, both from University of California, San Diego, in 1983 and 1988, respectively.

From 1988 to 1992, he worked as a Research Scientist, Manager, and Director of the Department of Electrooptic Engineering, Physical Optics Corporation, Torrance, CA. In 1992, he joined the University of Texas (UT), Austin, as a Faculty member, where he started the optical interconnect research program in the Electrical and Computer Engineering (ECE) Department. He holds the Cullen Trust for Higher Education Endowed Professorship at UT.